Polymeric Dopant Effects of Bent-Core Covalent-Bonded and Hydrogen-Bonded Structures on Banana-Shaped Liquid Crystalline Complexes

PO-JEN YANG, LING-YUNG WANG, CHIEH-YIN TANG, HONG-CHEU LIN

Department of Materials Science and Engineering, National Chiao Tung University, Hsinchu, Taiwan, Republic of China

Received 29 September 2009; accepted 3 November 2009
DOI: 10.1002/pola.23823
Published online in Wiley InterScience (www.interscience.wiley.com).

ABSTRACT: Two series of banana-shaped liquid crystalline (LC) H-bonded complexes **HP$_m$/CB$_n$** (i.e., bent-core H-bonded side-chain homopolymer **HP** mixed with bent-core covalent-bonded small molecule **CB**) and **CP$_m$/HB$_n$** (i.e., bent-core covalent-bonded side-chain homopolymer **CP** mixed with bent-core H-bonded small molecular complex **HB**) with various ***m/n*** molar ratios were developed. The bent-core covalent- and H-bonded structural moieties were homopolymerized in the banana-shaped LC H-bonded complexes **HP$_m$/CB$_n$** and **CP$_m$/HB$_n$**, respectively. The influences of ***m/n*** molar ratios (polymeric moieties vs. small molecular moieties) on the mesomorphic and electro-optical properties of both banana-shaped LC H-bonded complexes **HP$_m$/CB$_n$** and **CP$_m$/HB$_n$** were investigated. The polar smectic phases could be achieved and stabilized by smaller contents of polymeric dopants in banana-shaped LC H-bonded complexes, such as **HP1/CB10**, **HP1/CB15**, **CP1/HB10**, and **CP1/HB15**, which possessed tunable spontaneous polarization (*P*s) values according to the molar ratios of ***m/n***, that is, lower *P*s values obtained in H-bonded complexes **HP$_m$/CB$_n$** and **CP$_m$/HB$_n$** with higher ratios of H-bonded moieties (larger ***m/n*** molar ratios), respectively. © 2010 Wiley Periodicals, Inc. J Polym Sci Part A: Polym Chem 48: 764–774, 2010

KEYWORDS: ferroelectricity; liquid crystalline polymers; supramolecular structure

INTRODUCTION Liquid crystalline (LC) materials bearing banana-shaped mesogens become interesting topics duo their special electro-optical properties, such as spontaneous polarized capabilities and nonlinear optics.[1,2] On the basis of various intermolecular arrangements, several kinds of special mesophases in accordance with banana-shaped (or bent-core) molecular designs with particular mesophases, including columnar stacking, tilted smectic, and three-dimensional structures, named as B1–B7 phases were developed and identified.[3] Traditionally, electro-optical switching behaviors were observed in the smectic B1, B2, B5, and B7 phases, where the B2 (SmCP) phase had been prevailingly investigated. Depending on the polar direction and molecular tilted direction in neighboring layers of the SmCP phase, ferroelectric (F) and antiferroelectric (A) states possessed identical/inverse polarizations and synclinic (S)/anticlinic (A) arrangements with alike/opposite molecular tilted aspects between layer to layer, respectively. Hence, four kinds of different supramolecular architectures denoted SmC_AP_A, SmC_SP_A, SmC_AP_F, and SmC_SP_F were recognized as homochiral (SmC_AP_A and SmC_SP_F) and racemic (SmC_SP_A and SmC_AP_F) conditions separately.[4] With respect to the bent-core molecular architectures, the traditional banana-shaped liquid crystals were generally formed by two bent-substituted rigid arms connected to a central cyclic ring (through polar or nonpolar functional groups) with a suitable bent angle and linking, where appropriate lengths of flexible chains were attached.[5] Among these bent-shaped modeling frameworks, the structural variations of achiral molecular designs, such as the central parts,[6] lateral substituents,[7] linking groups,[8] terminal chains,[9] and the number of rings,[10] would affect their physical properties to different extents in small molecular systems. Recently, poly-molecular systems, that is, dimeric,[11] main-chain polymeric,[12] side-chain polymeric,[13] and dendritic structures,[14] were also developed to investigate the influence of molecular configurations on mesomorphic and electro-optical properties. Moreover, some novel supramolecular bent-core interactions or their nanocomposite architectures have been integrated into organic or inorganic parts to display special electro-optical characteristics, for instance, bent-core derivatives embedded with nanoparticles,[15] bent-core H-bonded supramolecules,[16,17] and bent-core structures with silyl and siloxyl linkages.[18]

To retain the electro-optical switching behavior in the bent-core structures is constantly the important assignment in the field of banana-shaped LC research. However, even if many kinds of bent-core small molecular systems displayed particular polar switching current behaviors, duo to the higher viscosities and larger inter-/intra-molecular interactions in polymers, such switching current behaviors were not easy to be obtained (or detected) in analogous bent-core polymer derivatives.[19–21] Interestingly, the switching current behavior of the SmCP phase in the monomeric units was sustained

Additional Supporting Information may be found in the online version of this article. Correspondence to: H.-C. Lin (E-mail: linhc@cc.nctu.edu.tw)
Journal of Polymer Science: Part A: Polymer Chemistry, Vol. 48, 764–774 (2010)

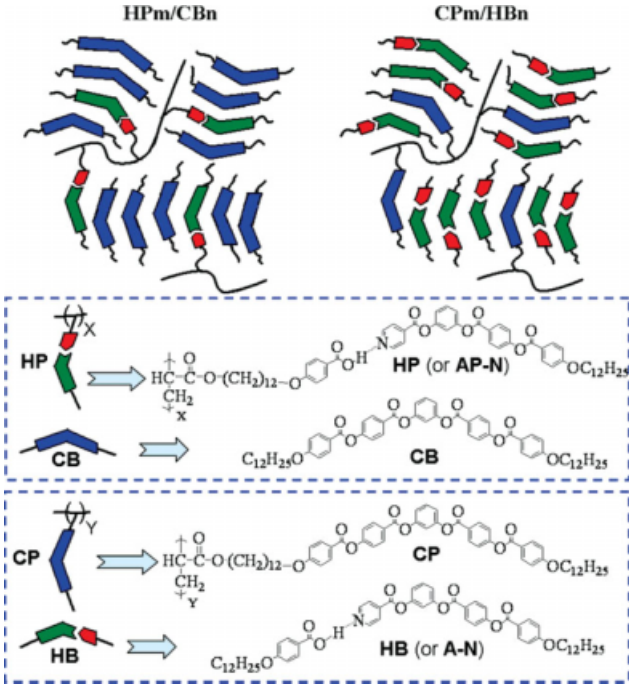

FIGURE 1 Chemical structures of banana-shaped LC H-bonded complexes $\mathbf{HP}_m/\mathbf{CB}_n$ and $\mathbf{CP}_m/\mathbf{HB}_n$ (where m/n = 15/1, 10/1, 15/1, 1/1, 1/5, 1/10, and 1/15) and their composing H-bonded and covalent-bonded bent-core side-chain homopolymers (**HP** and **CP**, respectively) as well as H-bonded and covalent-bonded bent-core small molecules (**HB** and **CB**, respectively).

and the ferro-electricity could be modified by the polymer structural design of dimethylsiloxane diluted polysiloxane side-chain copolymer frameworks.[13] According to the previous works, bent-core H-bonded small molecules could yield lower mesophasic transition temperatures, enthalpies, and threshold voltages than those of fully covalent-bonded five-ring banana-shaped molecular analogues and H-bonded side-chain polymeric derivatives, which suggested that softer bent-core intermolecular arrangements were present in both H-bonded and small molecular designs.[22–24] Regarding the small molecular systems containing two different fully covalent-bonded components, unusual molecular arrangements and mesomorphic behaviors were developed by blending rod-like liquid crystals with bent-core LC dopants.[25,26] Meanwhile, the blended polymeric systems (mainly side-chain polymers) were expanded by doping,[27] copolymerization,[28–33] and H-bonded complexation[34] with chiral/achiral LC components to induce the particular mesomorphic and electro-optical properties. In recent years, some related literatures about H-bonded polymeric materials and applications of block copolymers have been developed by Hawker's group.[35,36] In addition, the pioneering works of side-chain H-bonded LC polymers by Kato's groups have also been studied as well.[37–40]

As shown in Figure 1, to investigate the polymeric dopant effects of bent-core covalent- and H-bonded structures on the mesomorphic and electro-optical properties of banana-shaped LC complexes, two series of H-bonded complexes $\mathbf{HP}_m/\mathbf{CB}_n$ (i.e., bent-core H-bonded side-chain homopolymer **HP** mixed with bent-core covalent-bonded small molecule **CB**) and $\mathbf{CP}_m/\mathbf{HB}_n$ (i.e., bent-core covalent-bonded side-chain homopolymer **CP** mixed with bent-core H-bonded small molecular complex **HB**) with various m/n molar ratios (m/n = 15/1, 10/1, 15/1, 1/1, 1/5, 1/10, and 1/15) were developed. The mesomorphic and electro-optical properties of the H-bonded complexes were investigated and characterized by polarizing optical microscopy (POM), differential scanning calorimetry (DSC), powder X-ray diffraction (XRD), and electro-optical (EO) switching current experiments. Herein, the polar smectic (SmC_AP_A) phase with switching current behavior (or spontaneous polarization) was introduced and stabilized in some of the banana-shaped LC H-bonded complexes $\mathbf{HP}_m/\mathbf{CB}_n$ and $\mathbf{CP}_m/\mathbf{HB}_n$ by blending various m/n molar ratios of soft H-bonded bent-core moieties with rigid covalent-bonded bent-core moieties, where one of the moieties was homopolymerized as side-chain H-bonded homopolymer (**HP**) or covalent-bonded homopolymer (**CP**), respectively. Finally, their mesophasic ranges and spontaneous polarization (*Ps*) values could be adjusted by the m/n molar ratios (polymeric moieties vs. small molecular moieties) in the banana-shaped LC H-bonded complexes $\mathbf{HP}_m/\mathbf{CB}_n$ and $\mathbf{CP}_m/\mathbf{HB}_n$.

EXPERIMENTAL

Methods

^{1}H NMR spectra were recorded on a Varian Unity 300 MHz spectrometer using d_6-dioxane and $CDCl_3$ as solvents and mass spectra were determined on a Micromass TRIO-2000 GC-MS. Elemental analyses (EA) were performed on a Heraeus CHN-OS RAPID elemental analyzer. Gel permeation chromatography (GPC) analyses were conducted on a Waters 1515 separation module using polystyrene as a standard and THF as an eluant. Mesophasic textures were characterized by polarizing optical microscopy (POM) using a Leica DMLP equipped with a hot stage. Infrared (IR) spectra were investigated by Perk–Elmer Spectrum 100 instrument. Temperatures and enthalpies of phase transitions were determined by differential scanning calorimetry (DSC, model: Perkin Elmer Pyris 7) under N_2 at a heating and cooling rate of 10 °C/min. Synchrotron powder X-ray diffraction (XRD) measurements were performed at beamline BL17A of the National Synchrotron Radiation Research Center (NSRRC, Taiwan), where the wavelength of X-ray was 1.33366 Å. The powder samples were packed into a capillary tube and heated by a heat gun, whose temperature controller was programmable by a PC with a PID feedback system. The scattering angle theta was calibrated by a mixture of silver behenate and silicon. The electro-optical properties were determined in commercially available ITO cells (from Mesostate, thickness = 4.25 μm, active area = 1 cm^2) with rubbed polyimide alignment coatings (parallel rubbing direction). A digital oscilloscope (Tektronix TDS-3012B) was used in these measurements, and a high power amplifier connected to a function generator (GW Model GFG-813) with a d.c. power supply (Keithley 2400) was utilized in the d.c.

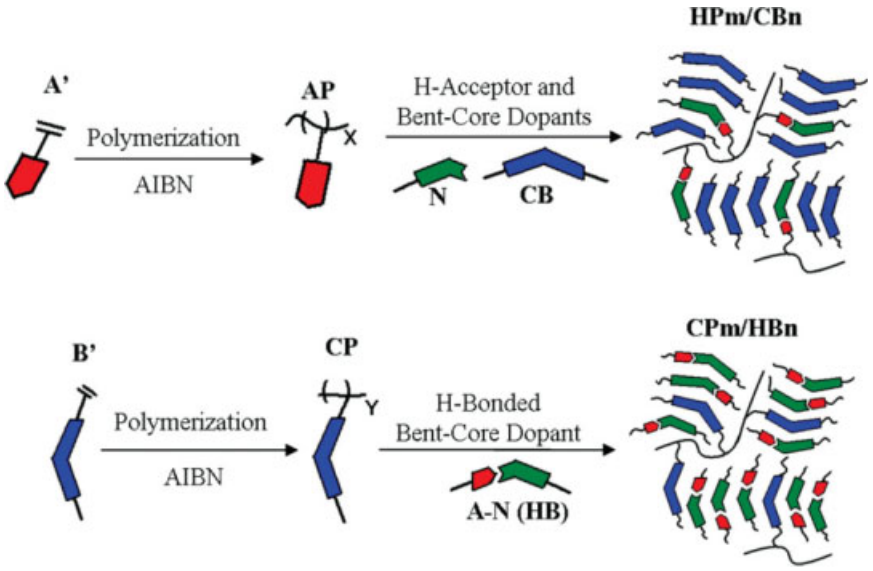

SCHEME 1 Homopolymerization and complexation of banana-shaped LC H-bonded complexes $\mathbf{HP}_m/\mathbf{CB}_n$ and $\mathbf{CP}_m/\mathbf{HB}_n$.

field experiments. During electro-optical measurements, the modulations of textures by applying electric fields were observed by POM.

Synthesis of Monomers

All synthetic procedures of monomers **A**′ (H-donor monomer) and **B**′ (bent-core covalent-bonded monomer) as well as pyridyl H-acceptor **N** are demonstrated in Scheme S1 of the supporting information. The synthetic details of all compounds in Scheme S1 are shown in the supporting information.

Synthesis of Polymers (H-Donor Homopolymer AP and Covalent-Bonded Homopolymer CP) and Preparation of H-Bonded Complexes ($\mathbf{HP}_m/\mathbf{CB}_n$ and $\mathbf{CP}_m/\mathbf{HB}_n$)

The side-chain proton donor (H-donor) homopolymer **AP** and bent-core covalent-bonded homopolymer **CP** were carried out by free radical coupling reactions of monomers **A**′ and **B**′, respectively, with initiator 2,2′-azobis-isobutyronitrile (AIBN) in Scheme 1. All reactions were proceeded in dry THF solvent under N_2 at the reflux temperature for 24 h. The accomplished organic liquid was dropped into strong stirring diethyl ether (EA) solvent to precipitate products, which were purified again by THF and EA to acquire pure compounds. The H-bonded complexes ($\mathbf{HP}_m/\mathbf{CB}_n$ and $\mathbf{CP}_m/\mathbf{HB}_n$) were constructed by blending appropriate molar ratios of proton donors **AP** (H-donor polymers) and acceptors **N** (H-acceptors) in the solutions of chloroform/THF (ca. 1:1 vol.), which were self-assembled into supramolecules by evaporating solvents slowly. Hence, two series of H-bonded complexes $\mathbf{HP}_m/\mathbf{CB}_n$ (**HP15/CB1**, **HP10/CB1**, **HP5/CB1**, **HP1/CB1**, **HP1/CB5**, **HP1/CB10**, and **HP1/CB15**) and $\mathbf{CP}_m/\mathbf{HB}_n$ (**CP15/HB1, CP10/HB1, CP5/HB1, CP1/HB1, CP1/HB5, CP1/HB10**, and **CP1/HB15**) with various ***m/n*** molar ratios (***m/n*** = 15/1, 10/1, 5/1, 1/1, 1/5, 1/10, and 1/15) were prepared as shown in Scheme 1.

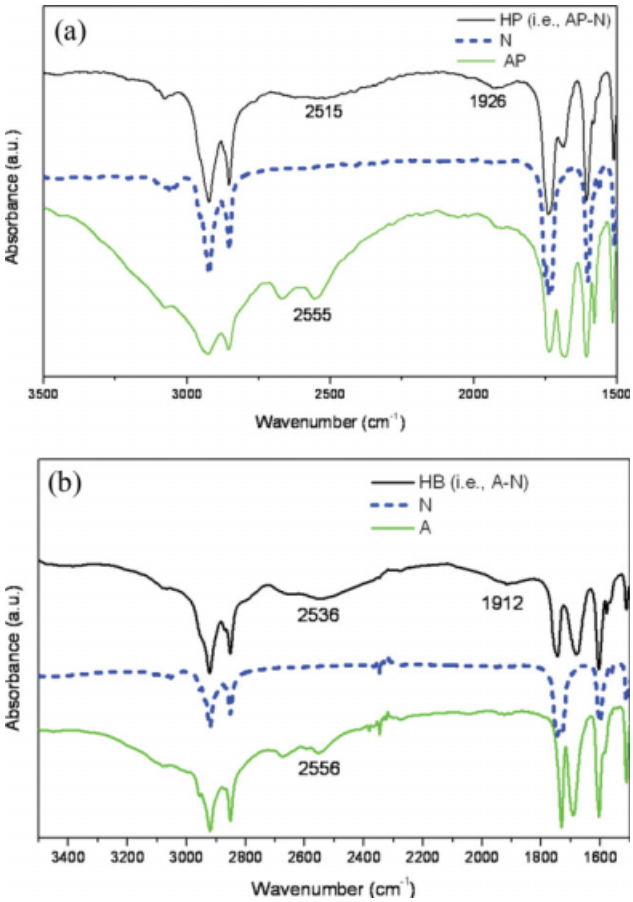

FIGURE 2 IR spectra of (a) H-bonded bent-core side-chain polymer complex **HP** and its components **N** (H-acceptor) and **AP** (H-donor homopolymer) and (b) H-bonded bent-core small molecular complex **HB** and its components **N** (H-acceptor) and benzoic acid derivative **A** (H-donor). [Color figure can be viewed in the online issue, which is available at www.interscience.wiley.com.]

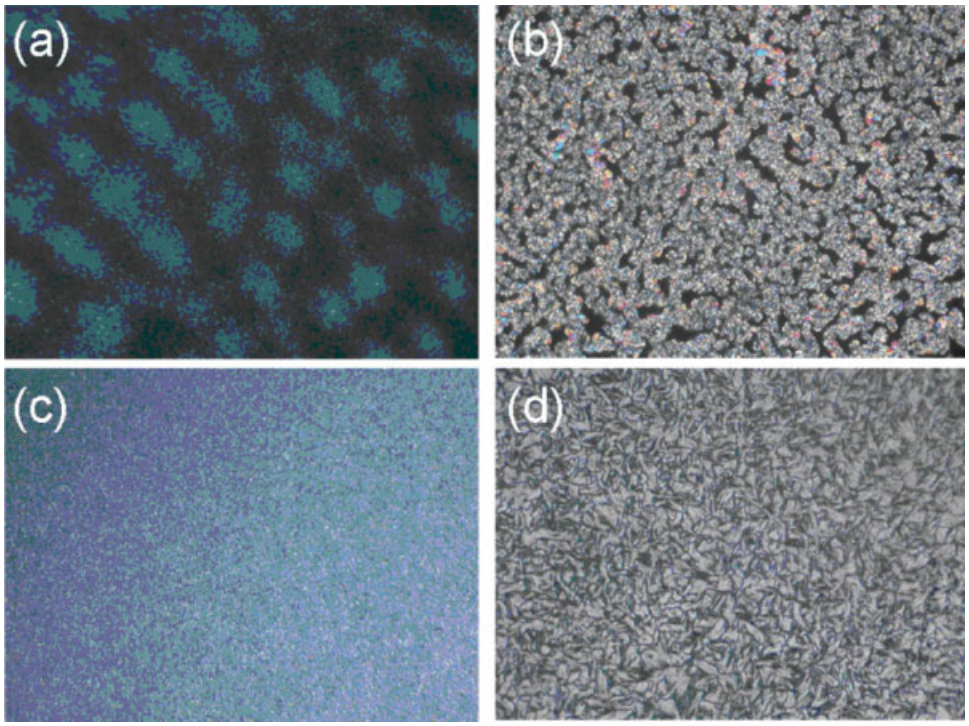

FIGURE 3 POM textures at the cooling process: (a) the tilted smectic phase with grainy domain and birefringence of H-bonded complex **HP5/CB1** at 100 °C; (b) the polar smectic phase with schlieren and fan-like textures of H-bonded complex **HP1/CB15** at 90 °C; (c) the tilted smectic phase with birefringence of H-bonded complex **CP1/HB5** at 80 °C; (d) the undefined SmXP phase with schlieren and fan-like textures of H-bonded complex **CP1/HB15** at 90 °C. [Color figure can be viewed in the online issue, which is available at www.interscience.wiley.com.]

RESULTS AND DISCUSSION

Polymer Characterization

To identify the chemical structures of all components in this study, the side-chain proton donor (H-donor) homopolymer **AP** and bent-core covalent-bonded homopolymer **CP** along with their corresponding monomeric moieties **A′** (H-donor monomer) and **B′** (bent-core covalent-bonded monomer) were characterized by ^{1}H NMR measurements. Both monomers **A′** and **B′** were confirmed by the resonant peaks in the chemical shift range of 5.7–6.4 ppm, which belong to the signals of acryl groups and demonstrate in Figure S1(a) of the supporting information. However, the chemical shift peaks in the range of 5.7–6.4 ppm were disappeared in the corresponding side-chain polymers **AP** and **CP** to prove the complete polymerization of monomers **A′** and **B′** [see Fig. S1(b)]. Compared with monomers **A′** and **B′**, the resonant peaks (a and b) of H-donor polymer **AP** in the range of 6.6 ppm to 8.5 ppm (attributed to aromatic rings) did not shift clearly, and the resonant peaks (c, d, e, f, g, h, and i) of bent-core covalent-bonded homopolymer **CP** belonged to the five bent-core benzoic rings as those of monomer **B′**. Furthermore, the number average molecular weights (M_n) and polydispersity index (PDI) values measured by GPC experiments for side-chain polymers **AP** and **CP** were 5.1×10^3 (with PDI = 1.13) and 12.7×10^3 (with PDI = 1.29), respectively.

IR Characterization

The existence and stability of H-bonds in side-chain polymeric H-bonded complex **HP** (i.e., **AP-N**: H-donor homopolymer **AP** supramolecularly complexed with H-acceptor **N**) and small molecular H-bonded complex **HB** (i.e., **A-N**: H-donor **A** supramolecularly complexed with H-acceptor **N**) were characterized by IR spectra. The IR spectra of H-bonded complexes **HP** (i.e., polymeric complex **AP-N**) and **HB** (i.e., small molecular complex **A-N**) and their corresponding H-acceptor **N**, H-donor **A**, and H-donor homopolymer **AP** in Figure 2 were compared to examine the existence of H-bonds. In contrast to the O-H band of pure H-donor homopolymer **AP** at 2555 cm^{-1} in Figure 2(a), weaker O-H bands observed at 2515 and 1926 cm^{-1} in side-chain polymeric H-bonded complex **HP** (i.e., **AP-N**) were indicative of hydrogen bonding between the acidic groups of H-donor homopolymer **AP** and the pyridyl groups of H-acceptor **N**.[41,42] As shown in Figure 2(b), the formation of H-bonds between H-donor **A** and H-acceptor **N** was also confirmed in small molecular H-bonded complex **HB** (i.e., **A-N**), where O-H bands of H-bonded complex **HB** observed at 2536 and 1912 cm^{-1} were weaker than that of pure H-donor **A** observed at 2556 cm^{-1}. These results suggested that supramolecular frameworks of H-bonded **HP** (i.e., **AP-N**) and **HB** (i.e., **A-N**) were formed by acid H-donor polymer **AP** and H-donor **A**, respectively, with pyridyl H-acceptor **N**.

Mesophasic and Thermal Properties of Banana-Shaped H-Bonded Complexes HP_m/CB_n and CP_m/HB_n

To investigate the polymeric dopant effects of covalent- and H-bonded structures on banana-shaped H-bonded complexes, the mesomorphic and thermal properties of H-bonded complexes HP_m/CB_n and CP_m/HB_n with various ***m/n*** molar ratios (i.e., 15/1, 10/1, 5/1, 1/1, 1/5, 1/10, and 1/15) were investigated by POM and DSC measurements. The thermal properties and phase behaviors of banana-shaped LC H-bonded complexes HP_m/CB_n and CP_m/HB_n are illustrated in Figures 3 and 4 and Tables 1 and 2. Banana-shaped H-bonded complexes HP_m/CB_n (i.e., bent-core H-bonded side-chain homopolymer **HP** mixed with bent-core covalent-

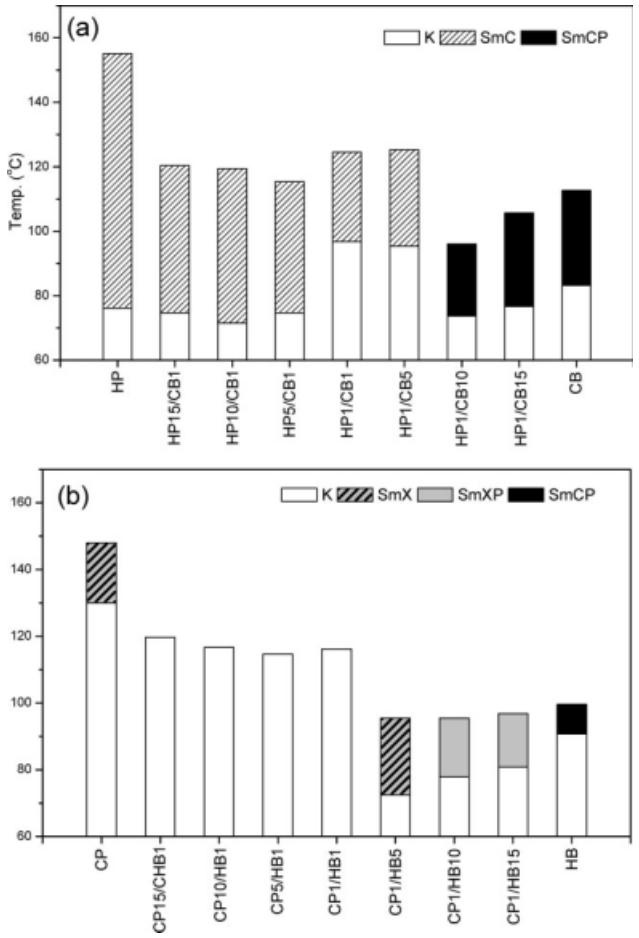

FIGURE 4 Phase diagrams (upon second cooling): (a) Banana-shaped H-bonded complexes $\mathbf{HP}_m/\mathbf{CB}_n$, consisting of side-chain H-bonded homopolymer **HP** (i.e., **AP-N**) and bent-core covalent-bonded molecule **CB** and (b) banana-shaped H-bonded complexes $\mathbf{CP}_m/\mathbf{HB}_n$, consisting of covalent-bonded side-chain homopolymer **CP** and H-bonded small molecular complex **HB**.

bonded small molecule **CB**) mostly possessed the enantiotropic tilted smectic (SmC) phases, which were verified by POM to show the grainy domain, schlieren, and fan-like textures. For instance, the grainy domain of H-bonded complex **HP5/CB1** is demonstrated in Figure 3(a), and H-bonded complexes $\mathbf{HP}_m/\mathbf{CB}_n$ (m/n = 15/1, 10/1, 5/1, 1/1, and 1/5) exhibited the similar mesophasic type to indicate the tilted smectic phase. Regarding H-bonded complexes **HP1/CB10** and **HP1/CB15** with low m/n molar ratios, an enantiotropic polar smectic C phase (SmCP) was obtained as that of bent-core covalent-bonded small molecule **CB**, but H-bonded complexes **HP1/CB10** and **HP1/CB15** possessed lower melting and isotropization temperatures. The schlieren and fan-like textures of H-bonded complex **HP1/CB15** as characteristic textures of the SmCP phase are shown in Figure 3(b). Comparing all phase transition temperatures of H-bonded complexes $\mathbf{HP}_m/\mathbf{CB}_n$ in Table 1 and Figure 4(a), side-chain H-bonded homopolymer **HP** (i.e., **AP-N**) revealed the highest isotropization temperatures and the widest mesophasic range (the SmC phase), and some H-bonded complexes $\mathbf{HP}_m/\mathbf{CB}_n$ (as m/n = 1/10 and 1/15) with less polymeric dopants exhibited lower isotropization temperatures than that of bent-core covalent-bonded molecule **CB** [see Fig. 4(a)]. In addition, only H-bonded complexes **HP1/CB10** and **HP1/CB15** doped with less polymeric configurations (alike bent-core covalent-bonded small molecule **CB**) would display the SmCP phase and the lowest isotropization temperatures. Therefore, the SmCP phase in bent-core compound **CB** was stabilized by H-bonded complexes $\mathbf{HP}_m/\mathbf{CB}_n$ (m/n = 1/10 and 1/15) with less H-bonded homopolymeric dopants, but it was replaced with the tilted smectic phase in H-bonded complexes $\mathbf{HP}_m/\mathbf{CB}_n$ (m/n = 15/1, 10/1, 5/1, 1/1, and 1/5) with higher amounts of polymeric frameworks, which was favored by bent-core H-bonded side-chain homopolymer **HP**.

With respect to banana-shaped H-bonded complexes $\mathbf{CP}_m/\mathbf{HB}_n$ (i.e., bent-core covalent-bonded side-chain homopolymer **CP** mixed with bent-core H-bonded small molecular complex **HB**), the mesophase was not clearly acquired in most H-bonded complexes $\mathbf{CP}_m/\mathbf{HB}_n$ (including m/n = 15/1, 10/1, 5/1, and 1/1). However, the birefringence of an enantiotropic tilted smectic phase was recovered in H-bonded complex **CP1/HB1** [see Fig. 3(c)]. In addition, the undefined polar smectic (SmXP) phase of H-bonded complexes **CP1/HB10** and **CP1/HB15** was acquired as that of bent-core H-bonded small molecular complex **HB** (i.e., **A-N**), which were clarified by the schlieren and fan-like textures of **CP1/HB15** as shown in Figure 3(d). Comparing the phase transition temperatures of H-bonded complexes $\mathbf{CP}_m/\mathbf{HB}_n$ and their corresponding components **CP** (bent-core covalent-bonded polymer) and **HB** (bent-core H-bonded molecular complex) illustrated in Table 2 and Figure 4(b), the isotropization temperatures of all H-bonded complexes $\mathbf{CP}_m/\mathbf{HB}_n$ were lower than that of polymer **CP**, and some H-bonded complexes $\mathbf{CP}_m/\mathbf{HB}_n$ (as m/n = 1/5, 1/10, and 1/15) with less polymeric dopants exhibited lower isotropization temperatures than that of H-bonded molecular complex **HB** [see Fig. 4(b)]. Therefore, the SmXP phase in bent-core H-bonded molecular complex **HB** was stabilized by H-bonded complexes $\mathbf{CP}_m/\mathbf{HB}_n$ (m/n = 1/10 and 1/15) with less polymeric dopants, but it was replaced with the tilted smectic phase or even became nonmesomorphic in H-bonded complexes $\mathbf{CP}_m/\mathbf{HB}_n$ (m/n = 15/1, 10/1, 5/1, 1/1, and 1/5) with higher amounts of polymeric frameworks.

Overall, due to the stronger intermolecular interactions and tighter stackings of covalent- and H-bonded bent-cores in homopolymers (**CP** and **HP**, respectively), bent-core homopolymers **CP** and HP had higher isotropization temperatures than their H-bonded complexes $\mathbf{HP}_m/\mathbf{CB}_n$ and $\mathbf{CP}_m/\mathbf{HB}_n$. The looser molecular stackings of H-bonded complexes $\mathbf{HP}_m/\mathbf{CB}_n$ and $\mathbf{CP}_m/\mathbf{HB}_n$ provided H-bonded complex systems (as m/n = 1/10 and 1/15 possessing less polymeric dopants) with suitable disordered arrangements of both covalent- and H-bonded structures to stabilize the polar smectic phases, which would induce lower transition temperatures (and possibly wider mesophasic ranges) as well as tunable *P*s values (to be shown later) in the proper polymeric molar ratios of banana-shaped H-bonded complexes.

TABLE 1 Phase Transition Temperatures and Enthalpies of Banana-Shaped H-Bonded Complexes, Side-Chain H-Bonded Homopolymer **HP** (i.e., **AP-N**), and Bent-Core Covalent-Bonded Molecule **CB**

Complex/ Compound	Phase Transition Temperature/°C [Enthalpy/kJ/g] Heating (up)/Cooling (down)
HP	**Cr** 96.3 (3.0) **SmC** 162.2 (22.4) **Iso**
	Iso 155.1 (−27.5) **SmC** 76.2 (−4.5) **Cr**
HP15/CB1	**Cr** 92.5 (4.7) **SmC** 120.1 (8.8) **Iso**
	Iso 120.4 (−13.1) **SmC** 74.7 (−3.7) **Cr**
HP10/CB1	**Cr** 91.5 (6.7) **SmC** 118.3 (10.5) **Iso**
	Iso 119.4 (−17.1) **SmC** 71.5 (−5.2) **Cr**
HP5/CB1	**Cr** 90.3 (14.5) **SmC** 117.6 (11.1) **Iso**
	Iso 115.4 (−20.1) **SmC** 74.7 (−11.0) **Cr**
HP1/CB1	**Cr** 98.3 (27.0) **SmC** 127.0 (10.0) **Iso**
	Iso 124.5 (−10.4) **SmC** 96.8 (−16.9) **Cr**
HP1/CB5	**Cr** 96.2 (24.8) **SmC** 128.3 (9.2) **Iso**
	Iso 125.3 (−12.7) **SmC** 95.4 (−13.7) **Cr**
HP1/CB10	**Cr** 97.8 (67.0) **SmCP** 118.2 (19.2) **Iso**
	Iso 96.1 (−16.9) **SmCP** 73.7 (−43.7) **Cr**
HP1/CB15	**Cr** 100.3 (46.3) **SmCP** 110.5 (14.8) **Iso**
	Iso 105.7 (−19.8) **SmCP** 76.7 (−47.9) **Cr**
CB	**Cr** 101.7 (73.5) **SmCP** 115.4 (44.2) **Iso**
	Iso 112.7 (−43.8) **SmCP** 83.3 (−73.7) **Cr**

The phase transitions were measured by DSC at the second cooling scan with a cooling rate of 5 °C/min.
Iso, isotropic state; **SmC**, tilted smectic phase; **SmCP**, polar smectic phase; **Cr**, crystalline state.

Powder XRD Analyses of Bent-Core H-Bonded Complexes HP_m/CB_n and CP_m/HB_n

The molecular organizations of banana-shaped H-bonded complexes $\mathbf{HP}_m/\mathbf{CB}_n$ and $\mathbf{CP}_m/\mathbf{HB}_n$ in different mesophases, especially the layered structures of the smectic phases, could be characterized by XRD measurements, and their results are demonstrated in Tables 3 and 4. The formations of bent-core H-bonded complexes were further confirmed by the different *d*-spacing values of the smectic phases from those of their constituents. For instance, new sharp XRD peaks indexed as (001) in the small angle region were obtained in bent-core H-bonded complexes $\mathbf{HP}_m/\mathbf{CB}_n$ and $\mathbf{CP}_m/\mathbf{HB}_n$, respectively. In addition, no separated diffraction peaks in H-bonded complexes $\mathbf{HP}_m/\mathbf{CB}_n$ and $\mathbf{CP}_m/\mathbf{HB}_n$ were observed to prove no phase separations occurred between their components. Wide angle diffuse peaks corresponding to a *d*-spacing value of 4.6 Å indicated that similar liquid-like in-plane orders with average intermolecular distances were prevalent inside the smectic layers of bent-core side-chain polymer complexes. As shown in Tables 3 and 4 (also see Figs. 5 and 6 and Fig. S2 of the supporting information), the *d*-spacing values of bent-core H-bonded complexes $\mathbf{HP}_m/\mathbf{CB}_n$ and $\mathbf{CP}_m/\mathbf{HB}_n$ were mostly longer than those of bent-core homopolymers (**HP** and **CP**) and small molecules (**CB** and **HB**) owing to the less tilted and looser arrangements of the mixtures from both H-bonded and covalent-bonded structures.

Generally, bent-core H-bonded complexes $\mathbf{CP}_m/\mathbf{HB}_n$ had larger *d*-spacing values than H-bonded polymer complexes $\mathbf{HP}_m/\mathbf{CB}_n$. This phenomenon of smaller *d*-spacing values in H-bonded polymer complexes $\mathbf{HP}_m/\mathbf{CB}_n$ might be explained by that the higher flexibility of bent-core H-bonded homopolymer **HP** and its larger compatibility with bent-core covalent-bonded small molecule **CB** to induce the better interactions and more compact stackings of both components, which also explained the better mesomorphic properties of H-bonded polymer complexes $\mathbf{HP}_m/\mathbf{CB}_n$ (with wider SmCP phasic ranges and more constituted complexes possessing the SmC phase) than those of H-bonded complexes $\mathbf{CP}_m/\mathbf{HB}_n$ demonstrated in Figure 4. In addition, several sharp peaks were accomplished in covalent-bonded polymer **CP** to mean the long range ordered smectic structure,[18] and H-bonded homopolymer **HP** displayed a sharp diffraction peak to reveal tilted molecular organization. The largest *d*-spacing value of H-bonded complexes $\mathbf{HP}_m/\mathbf{CB}_n$ and $\mathbf{CP}_m/\mathbf{HB}_n$ (d_1 = 42.0 Å for **HP1/CB10** and d_1 = 51.6 Å for **CP1/HB15**,

TABLE 2 Phase Transition Temperatures and Enthalpies of Banana-Shaped H-Bonded Complexes, Bent-Core Covalent-Bonded Side-Chain Homopolymer **CP**, and H-Bonded Small Molecular Complex **HB**

Complex/Compound	Phase Transition Temperature/°C [Enthalpy/kJ/g] Heating (up)/Cooling (down)
CP	**Cr** 136.3 (23.5) **SmX** 150[b] **Iso**
	Iso 148[b] **SmX** 130 (−19.4) **Cr**
CP15/HB1	**Cr** 124.2 (26.0) **Iso**
	Iso 119.7 (−27.6) **Cr**
CP10/HB1	**Cr** 122.6 (38.3) **Iso**
	Iso 116.7 (−39.9) **Cr**
CP5/HB1	**Cr** 119.9 (32.7) **Iso**
	Iso 114.7 (−28.5) **Cr**
CP1/HB1	**Cr** 121.8 (33.7) **Iso**
	Iso 116.2 (−27.2) **Cr**
CP1/HB5	**Cr** 83.3 (13.7) **SmX** 95.5 (19.4) **Iso**
	Iso 95.0 (−36.7) **SmX** 72.0 (−15.9) **Cr**
CP1/HB10	**Cr** 84.6 (19.1) **SmXP** 98.1 (39.8) **Iso**
	Iso 95.5 (−47.9) **SmXP** 77.8 (−19.5) **Cr**
CP1/HB15	**Cr** 89.2 (17.6) **SmXP** 99.3 (56.5) **Iso**
	Iso 96.8 (−45.2) **SmXP** 80.8 (−15.9) **Cr**
HB	**Cr** 107.2 (79.0) **SmCP** 110.1[a] **Iso**
	Iso 109.6 (−35.4) **SmCP** 90.7 (−16.2) **Cr**

The phase transitions were measured by DSC at the second cooling scan with a cooling rate of 5 °C/min.
Iso, isotropic state; **SmC**, tilted smectic phase; **SmX**, undefined nonpolar smectic phase; **SmXP**, undefined polar smectic phase; **Cr**, crystalline state.
[a] The enthalpy values of two overlapped transition peaks.
[b] The temperature was observed by POM.

TABLE 3 Powder XRD Data of Banana-Shaped H-Bonded Complexes and Their Corresponding Components

Complex/ Compound	Cooling Temperature (°C)	2θ	*d*-Spacing (Å)
HP	140	2.17	35.2
		4.40	17.4
HP15/CB1	110	2.00	38.2
		4.05	18.9
HP10/CB1	110	1.92	39.8
		3.84	19.9
HP5/CB1	105	1.90	40.2
		3.80	20.1
HP1/CB1	110	1.87	40.9
		3.76	20.3
HP1/CB5	110	1.84	41.5
		3.90	19.6
HP1/CB10	80	1.82	42.0
		3.72	20.7
HP1/CB15	90	1.96	39.0
		3.98	19.2
		6.00	12.7
CB	100	2.23	34.3
		4.41	17.3

respectively) were shorter than the theoretical length of small molecular H-bonded complex **HB** (about 58 Å) to indicate the tilted smectic arrangement of polymer H-bonded complexes $\mathbf{HP}_m/\mathbf{CB}_n$ and $\mathbf{CP}_m/\mathbf{HB}_n$. For example, the two-dimensional structures of the SmCP and undefined SmXP phases in bent-core H-bonded complexes **HP1/CB10** and **CP1/HB10** were also confirmed to be tilted smectic structures by the XRD results (see Figs. 5 and 6).

Electro-Optical Properties of Bent-Core Complexes $\mathbf{HP}_m/\mathbf{CB}_n$ and $\mathbf{CP}_m/\mathbf{HB}_n$

To evaluate the polar switching current properties of the polar smectic phases (including SmCP and SmXP phases) in all banana-shaped H-bonded complexes $\mathbf{HP}_m/\mathbf{CB}_n$ and $\mathbf{CP}_m/\mathbf{HB}_n$, respectively, the triangular wave method was applied to measure the switching current behavior (i.e., the spontaneous polarization) in parallel rubbing cells with a cell gap of 4.25 μm. Regarding the spontaneous polarization (*Ps*) behaviors of H-bonded complexes $\mathbf{HP}_m/\mathbf{CB}_n$, two current peaks per half-period of an applied triangular voltage were observed in the switching current response curves of the polar smectic phases in H-bonded complexes **HP1/CB10** and **HP1/CB15**. The *Ps* values of banana-shaped H-bonded complexes and their corresponding components are summarized in Table 5. The two-peak switching current response curve of H-bonded complex **HP1/CB15** in the SmCP phase is shown in Figure 7(a), where the characteristic behavior of a sequential electric response was due to a ferroelectric state switched into an antiferroelectric ground state and back to the opposite ferroelectric state again. These phenomena confirmed the $SmCP_A$ (A = anti-ferroelectric behavior) structure of the B2 phase in the bent-core H-bonded complex.[43] As shown in Figure S3 of the supporting information, the anti-ferroelectric behavior could also be confirmed by the electro-optical response of transmittance versus applied voltage for H-bonded complex **HP1/CB10** (as $f = 10$ Hz and $V_{pp} = 300$ V). As shown in Figure 7(b), the *Ps* values of 280 and 450 nC/cm^2 were saturated at high voltages ($V_{pp} > 200$ V) for H-bonded complexes **HP1/CB10** and **HP1/CB15**, respectively. Compared with H-bonded complexes, the saturated *Ps* value of 500 nC/cm^2 in **CB** (the bent-core covalent-bonded small molecule) was obtained at a much higher voltage above $V_{pp} = 320$ V in our previous study.[24] This might be explained by that the host system of covalent-bonded molecule **CB** doped with H-bonded polymer **HP** would reach saturated *Ps* values at lower voltages due to the softer bent-core mixed configurations in H-bonded complexes **HP1/CB10** and **HP1/CB15**. Comparing the *Ps* values of H-bonded complexes **HP1/CB10** (*Ps* = 280 nC/cm^2) and **HP1/CB15** (*Ps* = 450 nC/cm^2), which reasonably lay between those of covalent-bonded host molecule **CB** (*Ps* = 500 nC/cm^2) and H-bonded guest polymer **HP** (without *Ps*), the *Ps* value of H-bonded complex **HP1/CB10** was much affected and reduced by doping a small amount of H-bonded guest polymer **HP** (***m/n*** = 1/10). Moreover, the electro-optical properties in the SmC phase of H-bonded complexes $\mathbf{HP}_m/\mathbf{CB}_n$ with ***m/n*** ratios between 15/1 and 1/5 were proven to be no polar switching current responses under AC fields.

With respect to the *Ps* values of H-bonded complexes $\mathbf{CP}_m/\mathbf{HB}_n$, for instance, H-bonded complex **CP1/HB15** revealed two-peak switching current response curves in Figure 8(a)

TABLE 4 Powder XRD Data of Banana-Shaped H-Bonded Complexes and Their Corresponding Components

Complex/ Compound	Cooling Temperature (°C)	2θ	*d*-Spacing (Å)
CP	140	2.10	36.4
		3.14	24.3
		3.85	19.9
		4.48	17.1
		5.20	14.7
CP1/HB5	80	1.51	50.6
		2.40	31.8
		4.20	18.2
		5.08	15.1
CP1/HB10	90	1.80	42.5
		2.70	28.3
		4.49	17.1
		5.49	13.9
CP1/HB15	90	1.48	51.6
		2.38	32.1
		3.18	24.0
		4.94	15.5
HB	100	1.62	47.2

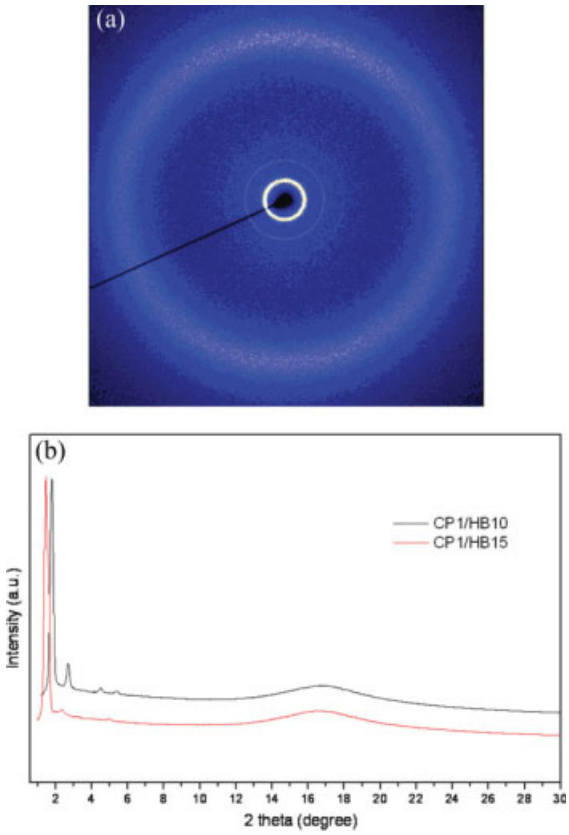

FIGURE 5 (a) Powder X-ray 2D pattern of H-bonded complex **HP1/CB10** (at 80 °C cooling) and (b) Powder X-ray diffraction intensities against angle profiles of H-bonded complexes **HP1/CB10** and **HP1/CB15** in the polar smectic phase (at 90 °C cooling). [Color figure can be viewed in the online issue, which is available at www.interscience.wiley.com.]

to prove the anti-ferroelectric behavior of the undefined polar smectic (SmXP) phase, and H-bonded complex **CP1/HB10** displayed a similar polar switching current behavior to indicate the existence of the $SmXP_A$ phase. As shown in Figure 8(b), the *Ps* values at high voltages (i.e., $V_{pp} > 200$ V) were both saturated at 350–355 nC/cm^2 for H-bonded complexes **CP1/HB15** and **CP1/HB10**. On the contrary, the saturated *Ps* value of 115 nC/cm^2 in bent-core H-bonded small molecular complex **HB** (i.e., **A-N**) was obtained at a higher voltage of $V_{pp} = 210$ V in our previous study.[24] Compared with the *Ps* values of H-bonded complexes **HP1/CB10** (*Ps* = 280 nC/cm^2) and **HP1/CB15** (*Ps* = 450 nC/cm^2) with analogous *m/n* molar ratios in Table 5, the *Ps* values of complexes **CP1/HB15** and **CP1/HB10** (*Ps* = 350 and 355 nC/cm^2, respectively) were surprisingly enhanced (much higher than those of their constituents, **HB** and **CP**), but the influence of *m/n* molar ratio on their *Ps* values was almost negligible. As revealed in Table 5, the higher *Ps* values of SmXP phase in bent-core H-bonded complexes **CP1/HB15** and **CP1/HB10** than that of H-bonded molecular complex **HB** indicated that the polar switching current behavior was not only contributed from H-bonded molecular complex **HB** but also provided by covalent-bonded polymer dopant **CP** (even though without *Ps*). Therefore, the mesophasic range, *Ps* value, and stability of the polar smectic phase could be much enhanced by doping H-bonded molecular complex **HB** with small molar ratios of bent-core covalent-bonded side-chain homopolymer **CP**.

A switching process could also be checked through the rotation of the extinction crosses (Fig. 9) by applying (or after removing) opposite d.c. electric fields in the banana-shaped H-bonded complexes with the SmCP phase. For instance, circular domains of H-bonded complex **HP1/CB15** were formed in the SmCP mesophasic range, in which the smectic layers were circularly arranged around the centers of the domains, which were organized according to the domain models proposed by Link and coworkers.[4,44] As shown in Figure 9, the rotation of the extinction crosses during the switched on and off states in H-bonded complex **HP1/CB15** demonstrated the chiral domain behavior.[10] In view of Figure 9(a,c), by applying d.c. electric fields (with reverse polarities), the extinction

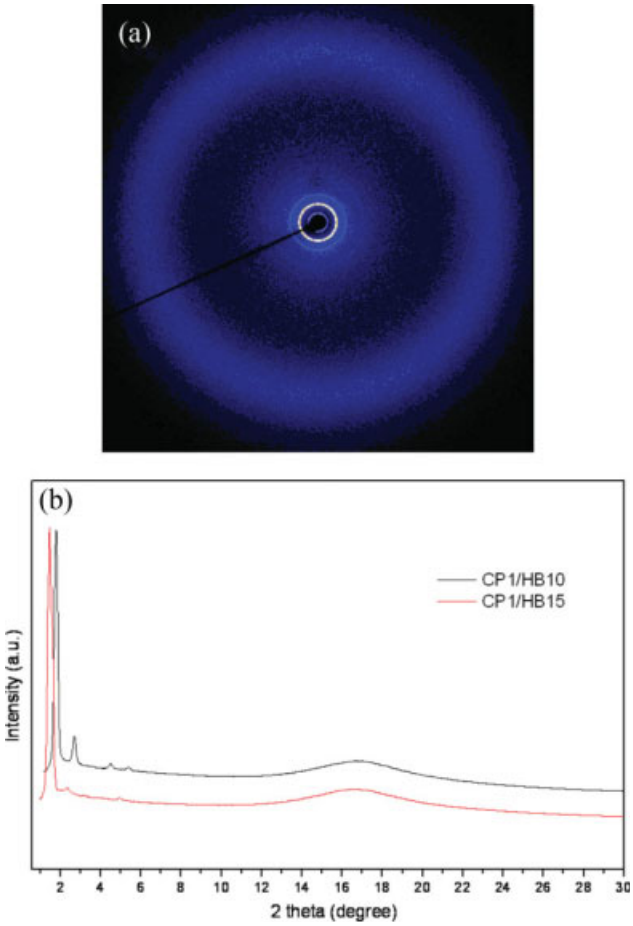

FIGURE 6 (a) Powder X-ray 2D pattern of H-bonded complex **CP1/HB10** (at 90 °C cooling) and (b) Powder X-ray diffraction intensities against angle profiles of H-bonded complexes **CP1/HB10** and **CP1/HB15** in the undefined polar smectic (SmXP) phase (at 90 °C cooling). [Color figure can be viewed in the online issue, which is available at www.interscience.wiley.com.]

TABLE 5 *P*s Values of Banana-Shaped H-Bonded Complexes and Their Corresponding Components

Complex/Compound	*P*s Value (nC/cm^2)[a]	Temperature (°C)
CB	500	100
HP1/CB15	450	90
HP1/CB10	280	80
HB	115	100
CP1/HB15	350	90
CP1/HB10	355	90

[a] The highest saturated *P*s values.

crosses rotated either counterclockwise or clockwise (i.e., rotated oppositely with positive and negative fields), indicating a synclinic tilt in the ferroelectric state (SmC_SP_F). By removing electric fields (off state), the extinction crosses were reoriented back to the crossed polarizer directions [see Fig. 9(b)], where an anticlinic tilt existed in the antiferroelectric ground state (SmC_AP_A). Hence, the anti-clinic and antiferroelectric polar smectic (SmC_AP_A) arrangement in the ground state of H-bonded complex **HP1/CB15** were identified, and the other H-bonded complexes possessing the antiferroelectric polar smectic (SmC_AP_A) phase were also confirmed.

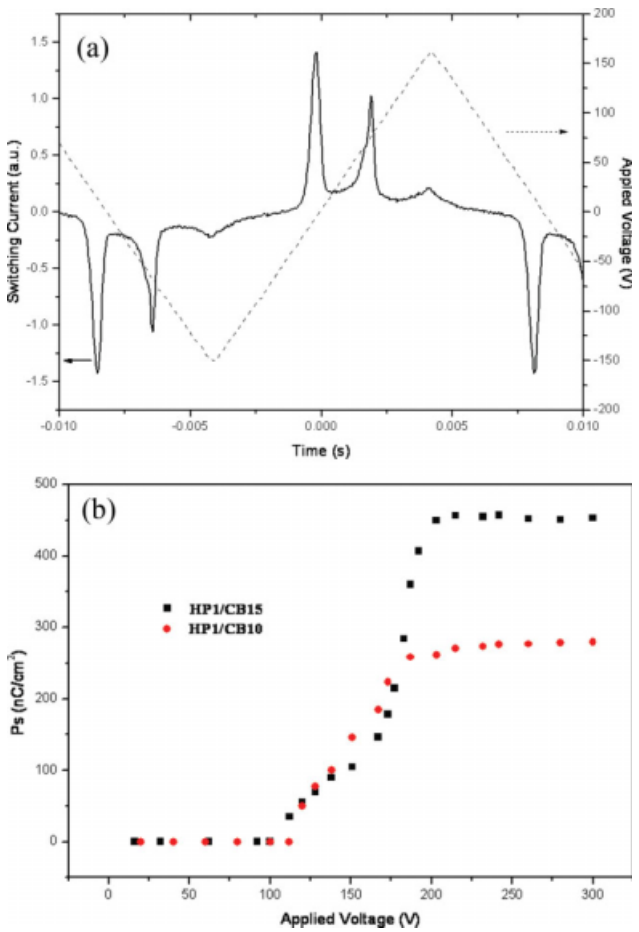

FIGURE 7 (a) Switching current responses of banana-shaped H-bonded complex **HP1/CB15** (at 80 °C cooling) under the triangular wave method (as V_{pp} = 300 V and f = 60 Hz). (b) *P*s values as a function of applied voltages (as f = 200 Hz) in the SmCP phase of banana-shaped H-bonded complexes **HP1/CB15** and **HP1/CB10** (at 90 °C cooling). [Color figure can be viewed in the online issue, which is available at www.interscience.wiley.com.]

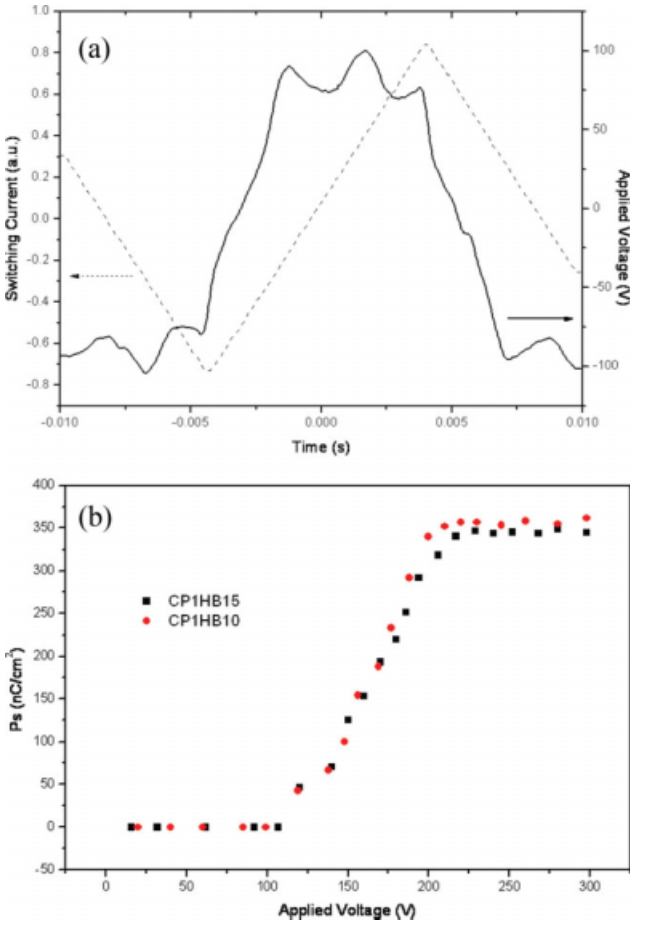

FIGURE 8 (a) Switching current responses of banana-shaped H-bonded complex **CP1/HB15** (at 85 °C cooling) under the triangular wave method (as V_{pp} = 210 V and f = 200 Hz). (b) *P*s values as a function of applied voltages (as f = 200 Hz) in the SmXP phase of banana-shaped H-bonded complexes **CP1/HB15** and **CP1/HB10** (at 90 °C cooling). [Color figure can be viewed in the online issue, which is available at www.interscience.wiley.com.]

The chiral domain behavior could also be proven by the method of rotating the polarizer without applying electric fields. For example, the polarizer was rotated clockwise by a small angle of 10° from the crossed position in complex **HP1/CB15**, then the dark and bright domains become clearly distinguishable [see Fig. 10(a)]. On rotating the polarizer counterclockwise by the same angle (10°) from the crossed position, the previously observed dark domains turned to bright domains, and vice versa [see Fig. 10(b)]. This observation was also indicative of the occurrence of chiral domains with opposite handedness.

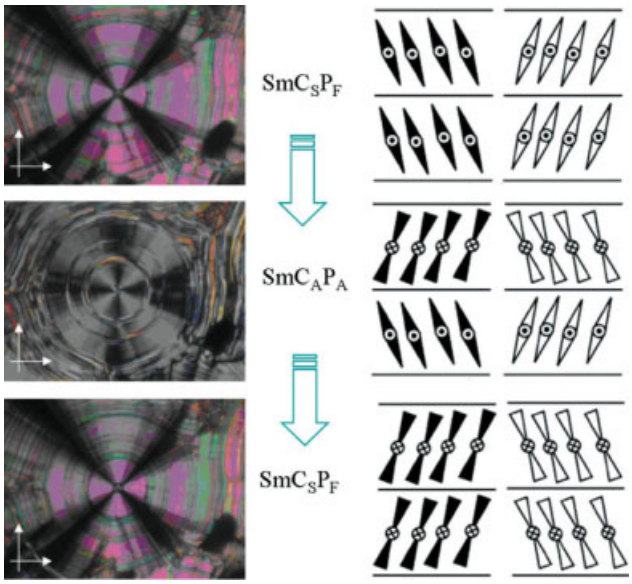

FIGURE 9 POM textures of the anti-ferroelectric SmC_AP_A chiral domain (in a parallel rubbing cell with a cell gap of 4.25 μm, where white arrows are the directions of polarizers and analyzers) in banana-shaped H-bonded complex **HP1/CB15** by applying d.c. electric fields from (a) −30 V → (b) 0 V → (c) +30 V (at 90 °C cooling). [Color figure can be viewed in the online issue, which is available at www.interscience.wiley.com.]

CONCLUSIONS

In summary, banana-shaped LC H-bonded complexes $\mathbf{HP}_m/\mathbf{CB}_n$ and $\mathbf{CP}_m/\mathbf{HB}_n$ (with various m/n molar ratios) were developed by mixing both H-bonded and covalent-bonded moieties in combination with polymeric and small molecular structures, where either H-bonded or covalent-bonded structural units were homopolymerized in the banana-shaped side-chain H-bonded LC polymer complexes $\mathbf{HP}_m/\mathbf{CB}_n$ and $\mathbf{CP}_m/\mathbf{HB}_n$, respectively, to stabilize the polar smectic phases. Because of the stronger intermolecular interactions and tighter stackings of H-bonded and covalent-bonded bent-cores in homopolymers (**HP** and **CP**), bent-core homopolymers **HP** and **CP** had higher isotropization temperatures than their H-bonded complexes $\mathbf{HP}_m/\mathbf{CB}_n$ and $\mathbf{CP}_m/\mathbf{HB}_n$, respectively. The looser molecular stackings of H-bonded complexes $\mathbf{HP}_m/\mathbf{CB}_n$ and $\mathbf{CP}_m/\mathbf{HB}_n$ provided H-bonded complex systems (as m/n = 1/10 and 1/15 possessing less polymeric dopants) with suitable disordered arrangements of both covalent- and H-bonded structures to stabilize the polar smectic phases (the SmCP and SmXP phases), which would induce lower transition temperatures (and possibly wider mesophasic ranges) as well as tunable *P*s values in the proper polymeric molar ratios of banana-shaped H-bonded complexes. Hence, lower *P*s values were obtained in H-bonded complexes $\mathbf{HP}_m/\mathbf{CB}_n$ and $\mathbf{CP}_m/\mathbf{HB}_n$ with higher ratios of H-bonded moieties (larger m/n molar ratios), correspondingly. Because of the higher flexibility of bent-core H-bonded homopolymer **HP** and its larger compatibility with bent-core covalent-bonded small molecule **CB** to induce the better interactions and more compact stackings of both components, the better mesomorphic properties of H-bonded polymer complexes $\mathbf{HP}_m/\mathbf{CB}_n$ (with wider SmCP phasic ranges and more constituted complexes possessing the SmC phase) than those of H-bonded complexes $\mathbf{CP}_m/\mathbf{HB}_n$. According to the XRD measurements and switching current responses (including the chirality investigation), the polar smectic phases (including the SmCP and undefined SmXP phases) were verified to be achieved and stabilized by smaller contents of polymeric dopants in banana-shaped LC H-bonded complexes, such as **HP1/CB10**, **HP1/CB15**, **CP1/HB10**, and **CP1/HB15**. Overall, the mesomorphic and electro-optical properties of banana-shaped LC materials could be efficiently adjusted by mixing either H-bonded or covalent-bonded bent-core side-chain homopolymers with low molecular weight bent-core LC materials possessing covalent-bonded or H-bonded designs opposite to the previous homopolymers.

The authors thank the financial support from the National Science Council of Taiwan (ROC) through NSC 96-2113-M-009-015. They also thank the National Center for High-performance Computing for computer time and facilities. The powder XRD measurements were supplied by beamline BL17A (charged by Jey-Jau Lee) of the National Synchrotron Radiation Research Center (NSRRC) in Taiwan.

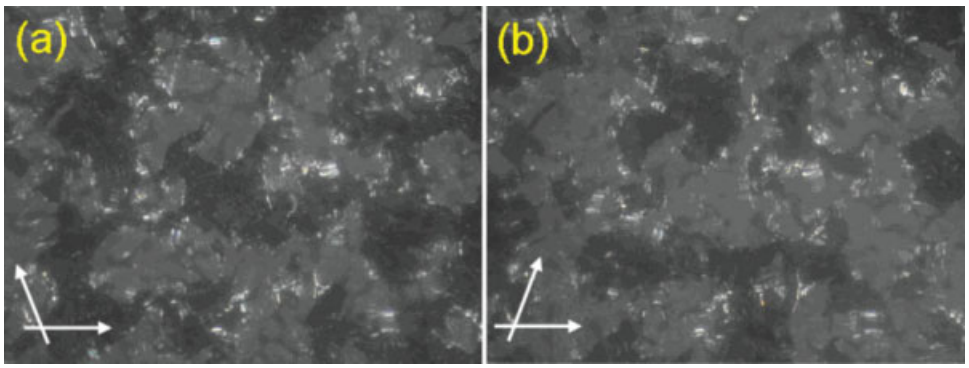

FIGURE 10 Chiral domain textures of H-bonded complex **HP1/CB15**. (Arrows are the directions of polarizers and analyzers). [Color figure can be viewed in the online issue, which is available at www.interscience.wiley.com.]

REFERENCES AND NOTES

1 Takezoe, H.; Takanishi, Y. Jpn J Appl Phys 2006, 597–625.

2 Nakata, M.; Shao, R. F.; Maclennan, J. E.; Weissflog, W.; Clark, N. A. Phys Rev Lett 2006, 96, 067802–067804.

3 Pelzl, G.; Diele, S.; Weissflog, W. Adv Mater 1999, 11, 707–724.

4 Link, D. R.; Natale, G.; Shao, R.; Maclennan, J. E.; Clark, N. A.; Korblova, E.; Walba, D. M. Science 1997, 278, 1924–1927.

5 Reddy, R. A.; Tschierske, C. J Mater Chem 2006, 16, 907–961.

6 Shen, D.; Diele, S.; Pelzl, G.; Wirth, I.; Tschierske, C. J Mater Chem 1999, 9, 661–672.

7 Dantlgraber, G.; Shen, D.; Diele, S.; Tschierske, C. Chem Mater 2002, 14, 1149–1158.

8 Anand, S.; Krishnan, R.; Weissflog, W.; Pelzl, G.; Diele, S.; Kresse, H.; Vakhovskaya, Z.; Friedemann, R. Phys Chem Chem Phys 2006, 8, 1170–1177.

9 Pelzl, G.; Tamba, M. G.; Sonja, F. T.; Schroder, M. W.; Baumeister, U.; Diele, S.; Weissflog, W. J Mater Chem 2008, 18, 3017–3031.

10 Shen, D.; Pegenau, A.; Diele, S.; Wirth, I.; Tschierske, C. J Am chem Soc 2000, 122, 1593–1601.

11 Umadevi, S.; Sadashiva, B. K.; Murthy, H. N. S.; Raghunathan, V. A. Soft Matter 2006, 2, 210–214.

12 Barbera, J.; Gimeno, N.; Monreal, L.; Pinol, R.; Ros, M. B.; Serrano, J. L. J Am Chem Soc 2004, 126, 7190–7191.

13 Keith, C.; Reddy, R. A.; Tschierske, C. Chem Commun 2005, 871–873.

14 Hahn, H.; Keith, C.; Lang, H.; Reddy, R. A.; Tschierske, C. Adv Mater 2006, 18, 2629–2633.

15 Marx, V. M.; Girgis, H.; Heiney, P. A.; Hegmann, T. J Mater Chem 2008, 18, 2983–2994.

16 Gimeno, N.; Ros, M. B.; Serrano, J. L.; Fuente, M. R. de la. Angew Chem Int Ed 2004, 43, 5235–5238.

17 Gimeno, N.; Ros, M. B.; Serrano, J. L.; Fuente, R. D. Chem Mater 2008, 20, 1262–1271.

18 Keith, C.; Reddy, R. A.; Hauser, A.; Baumeister, U.; Tschierske, C. J Am Chem Soc 2006, 128, 3051–3066.

19 Chen, X. F.; Tenneti, K. K.; Li, C. Y.; Bai, Y. W.; Wan, X. H.; Fan, X. H.; Zhou, Q. F.; Rong, L.; Hsiao, B. S. Macromolecules 2007, 40, 840–848.

20 Choi, E. J.; Ahn, J. C.; Chien, L. C.; Lee, C. K.; Zin, W. C.; Kim, D. C.; Shin, S. T. Macromolecules 2004, 37, 71–78.

21 Tenneti, K. K.; Chen, X. F.; Li, C. Y.; Shen, Z. H.; Wan, X. H.; Fan, X. H.; Zhou, Q. F.; Rong, L.; Hsiao, B. S. Macromolecules 2009, 42, 3510–3517.

22 Barbera, J.; Gimeno, N.; Pintre, I.; Ros, M. B.; Serrano, J. L. Chem Commun 2006, 1212–1214.

23 Schroder, M. W.; Diele, S.; Pelzl, G.; Weissflog, W. ChemPhysChem 2004, 5, 99–103.

24 Wang, L. Y.; Chiang, I. H.; Yang, P. J.; Li, W. S.; Chao, I. T.; Lin, H. C. J Phys Chem B 2009, 113, 14648–14660.

25 Nair, G.; Bailey, C. A.; Taushanoff, S.; Katalin, F. C.; Vajda, A.; Varga, Z.; Bota, A.; Jakli, A. Adv Mater 2008, 20, 3138–3142.

26 Kishikawa, K.; Muramatsu, N.; Kohmoto, S.; Yamaguchi, K.; Yamamoto, M. Chem Mater 2003, 15, 3443–3449.

27 Barmatov, E. B.; Bobrovsky, A. Y.; Pebalk, D. A.; Barmatova, M. V.; Shibaev, V. P. J Polym Sci Part A: Polym Chem 1999, 37, 3215–3225.

28 Liu, J. H.; Hung, H. J.; Yang, P. C.; Tien, K. H. J Polym Sci Part A: Polym Chem 2008, 46, 6124–6228.

29 Liu, J. H.; Yang, P. C.; Chiu, Y. H.; Suda, Y. J Polym Sci Part A: Polym Chem 2007, 45, 2026–2037.

30 Gao, L. C.; Fan, X. H.; Shen, Z. H.; Chen, X. F.; Zhou, Q. F. J Polym Sci Part A: Polym Chem 2009, 47, 319–330.

31 Lee, M. J.; Ji, H. N.; Han, Y. K. J Polym Sci Part A: Polym Chem 2008, 46, 6734–6745.

32 Shibaev, V.; Medvedev, A.; Bobrovsky, A. J Polym Sci Part A: Polym Chem 2008, 46, 6532–6541.

33 Gao, L. C.; Pan, Q. W.; Wang, C.; Yi, Y.; Chen, X. F.; Fan, X. H.; Zhou, Q. F. J Polym Sci Part A: Polym Chem 2007, 45, 5949–5956.

34 Vera, F.; Almuzara, C.; Orera, I.; Barbera, J.; Oriol, L.; Serrano, J. L.; Sierra, T. J Polym Sci Part A: Polym Chem 2008, 46, 5528–5541.

35 Tang, C.; Lennon, E. M.; Fredrickson, G. H.; Kramer, E. J.; Hawker, C. J. Science 2008, 322, 429–432.

36 Feldman, K. E.; Kade, M. J.; de Greef, T. F. A.; Meijer, E. W.; Kramer, E. J.; Hawker, C. J. Macromolecules 2008, 41, 4694–4700.

37 Kato, T.; Frechet, J. M. J Macromol Symp 1995, 98, 311–326.

38 Kato, T.; Frechet, J. M. J. J Am Chem Soc 1989, 111, 8533–8534.

39 Kato, T.; Frechet, J. M. J Macromolecules 1989, 22, 3818–3819.

40 Kato, T.; Kihara, H.; Uryu, T.; Fujishima, A.; Frechet, J. M. J Macromolecules 1992, 25, 6836–6841.

41 Wu, C. W.; Lin, H. C. Macromolecules 2006, 39, 7985–7997.

42 Lin, H. C.; Sheu, H. Y.; Chang, C. L.; Tsai, C. J Mater Chem 2001, 11, 2958–2965.

43 Zenyoji, M.; Takanishi, Y.; Ishikawa, K.; Thisayukta, J.; Watanabe, J.; Takezoe, H. J Mater Chem 1999, 9, 2775–2778.

44 Walba, D. M.; Korblova, E.; Shao, R.; Maclennan, J. E.; Link, D. R.; Glaser, M. A.; Clark, N. A. Science 2000, 288, 2181–2184.